ATLAS Internal Note
INDET-NO-188
14 November 1997

A Comparative Study of Reduced Layouts of the ATLAS Inner Detector

Dario Barberis, John Baines, Igor Gavrilenko, Stephen Haywood, Fred Luehring, Joleen Pater, Andrew Pickford, Alan Poppleton, Eduardo Ros, Alexander Rozanov, Giorgos Stavropoulos

Fabiola Gianotti, Luc Poggioli, Stefan Simion

Abstract

The performances of reduced Inner Detector layouts are compared to the performance of the full layout presented in the Inner Detector Technical Design Report. Three layouts have been fully simulated: a "new" TDR layout, with a material distribution as described in volume 2 of the TDR, a "new" layout with only 2 pixel layers and one with only 3 SCT layers. Reconstruction is performed with modified versions of the xKalman and iPatRec programs. Results are presented (without and with high luminosity pile-up) for the study of b-tagging, using $H \rightarrow b\bar{b}$ and $H \rightarrow u\bar{u}$ events with $m_H = 400$ GeV/c^2. The b-tagging performance is degraded by ~30% if a pixel layer is removed and by ~10% if an SCT layer is removed.The consequences of these degradations are explored for several physics studies. In particular, the loss of significance for WH ($H \rightarrow b\bar{b}$) from removing a pixel layer is ~6% and ~2% for an SCT layer. In the light of inevitable losses of performance from reduced detector efficiency and pile-up, further loss of performance resulting from a change of layout is undesirable.

1 Introduction

The pixel B-layer is now accepted as a permanent addition to the Inner Detector (ID). This represents an increase in the number of tracking layers, with a corresponding increase in the amount of material in the Inner Detector. This means an increase of the interaction probability of charged and neutral particles and therefore of the number of particles produced in these interactions. There is also concern expressed by the ATLAS calorimeter community and the LHCC that the ID material is at the upper end of what can be considered as acceptable in front of the calorimeters [1]. While it was thought that the removal of a precision tracking layer might improve the performance of the calorimeter, the purpose of this note is to evaluate the consequences of such a removal for physics with the Inner Detector and for ATLAS as a whole.

The most challenging pattern recognition study addressed in the ID TDR concerns the reconstruction and subsequent tagging of $H \rightarrow b\bar{b}$ and $H \rightarrow u\bar{u}$ with m_H = 400 GeV/c^2 [2]. In this note, we report on a update of that study with various reduced layouts. To facilitate a comparison of the pattern recognition capabilities of these layouts, only the minimum necessary set of changes have been made from the TDR reconstruction and analysis procedures [3].

The next section describes the layouts which have been simulated and the data sets which have been produced. Then we present the comparison of the b-tagging performances of the different layouts and their implications for ATLAS physics. In the following sections we summarise the other consequences on Inner Detector and Calorimeter performance. Finally we conclude with some comments on the overall performance of ATLAS.

2 Description of Layouts

The baseline layout is the “TDR” layout [4], consisting of 7 precision layers (3 pixel and 4 SCT), as defined in September 1996. Between that time and the publication of the Inner Detector TDR, the designs of a few parts of the Inner Detector systems were modified, as summarised in ref.[5]. Although we believed that these modifications would not affect the performance in any significant way, we have upgraded the simulation to take these changes into account.

2.1 Upgrades to the Baseline Layout

The differences between the “TDR” version of the simulation and the June 1997 version are listed below:

- the average material in the pixel barrels (disks) has been increased from 1.39% (0.94%) of a radiation length to 1.63% (1.63%) X_0 [6];
- the sign of the β-tilt angle (the angle between the normal to each module and the radial direction in the x-y plane) of the barrel pixels has been changed;
- the B-layer services have been routed along the beam pipe and then out in front of the end-cap cryostat;
- GaAs has been replaced by silicon in the inner rings of the SCT wheels;

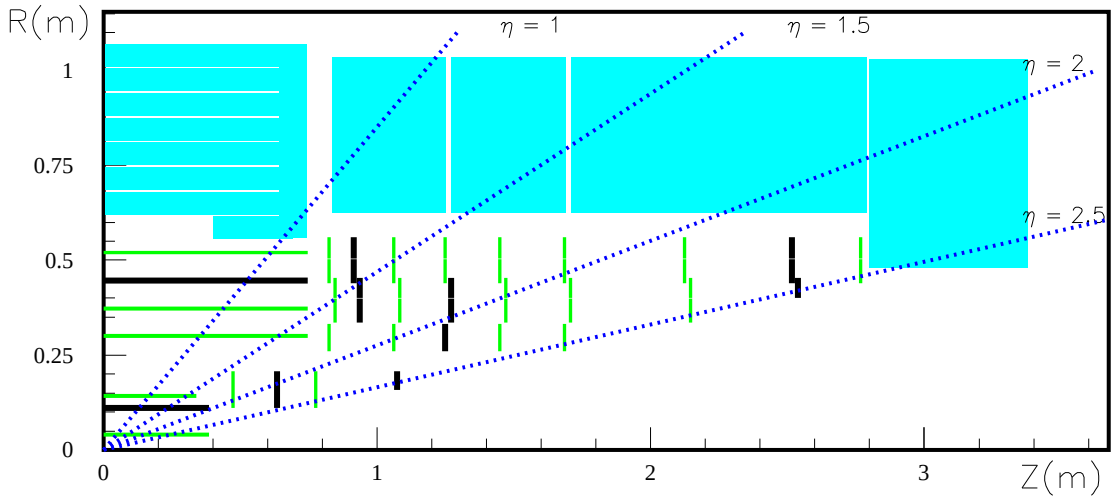

Figure 2-1 Schematic diagram of the Inner Detector baseline layout. The detectors shown in bold had their digits suppressed for the "2*+4" layout (pixels) and the "3+3*" layout (SCT) respectively.

- the thickness of the material at the outer radius of the end-cap TRT straws has been increased by 5% X_0.

The main effect of these changes is an increase of material at low radius (pixels) and large radius (TRT), accompanied by a more even distribution of the Inner Detector material as a function of η. Another effect is a small improvement in point resolution of the barrel pixel detector – a consequence of the smaller average cluster size in R-φ, due to the combined effect of the β-tilt and the Lorentz angle. In the following, this layout will be referred to as the "new TDR" layout. This layout is currently used for all on-going simulations.

2.2 Reduced Layouts

For the comparative study of b-tagging performance, we have used two different approaches:

1. following the procedure introduced in ref.[7], the data sets produced with the "TDR" layout have been analysed in three ways:
    a. as they are: results of this analysis are presented under the heading "3+4*";
    b. suppressing all digits from the 2nd pixel barrel and the 2nd and 4th pixel disks ("2*+4"); this is equivalent to removing the information from one out of three pixel layers over the full η coverage;
    c. suppressing all digits from the 3rd SCT barrel, the 2nd and 8th SCT wheels and the inner and middle ring of the 4th SCT wheel ("3+3*"; sometimes referred to as "3+4-1"); this is equivalent to removing the information from one out of four SCT layers over the full η coverage.

    In cases b) and c), the secondary tracks originating from the suppressed layer have not been considered for the analysis. Nevertheless, all tracks crossing the inactive material are subject to multiple scattering and interactions. Multiple scattering in the inactive material is taken into account by the track reconstruction procedures. Figure 2-1 shows the "TDR"

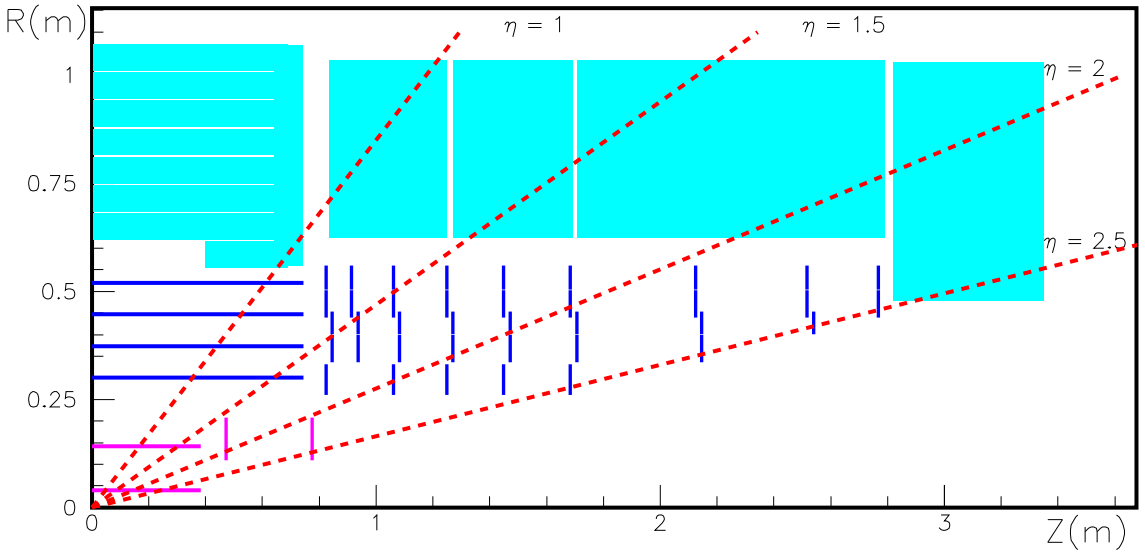

Figure 2-2 Schematic diagram of the Inner Detector “2+4” layout.

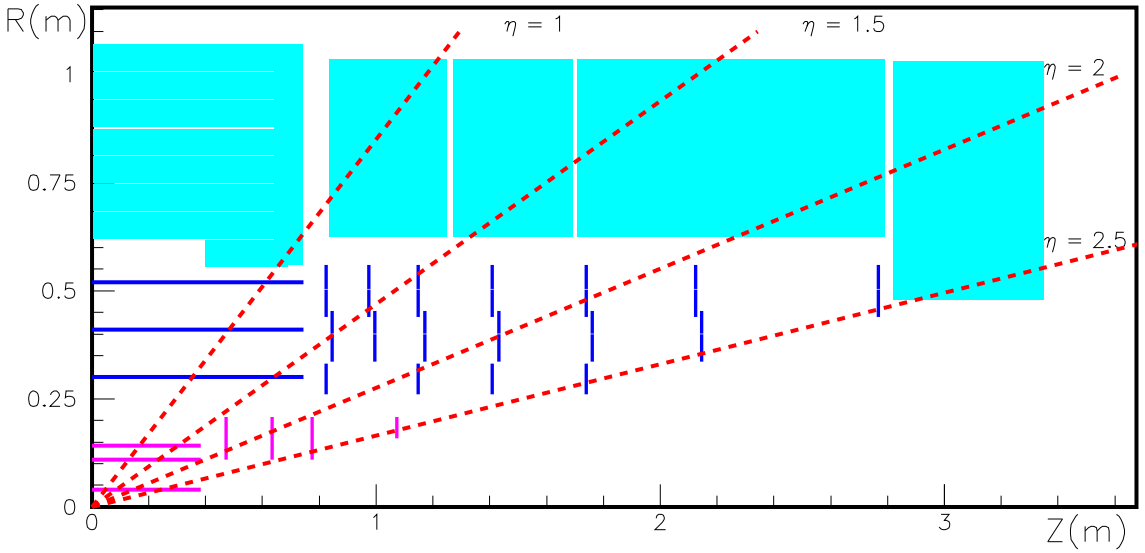

Figure 2-3 Schematic diagram of the Inner Detector “3+3” layout.

layout; the detectors shown in bold had their digits suppressed for the “2*+4” layout (pixels) and the “3+3*” layout (SCT) respectively.

2. new data sets have been generated with the “new TDR” geometry:
   a. with the default (“3+4”) layout;
   b. with a layout without the 2nd pixel barrel, the 2nd and 4th pixel disks and their services (“2+4”), see Figure 2-2;
   c. with an optimised layout with only 3 equally spaced SCT barrels and 7 SCT wheels (“3+3”), see Figure 2-3.

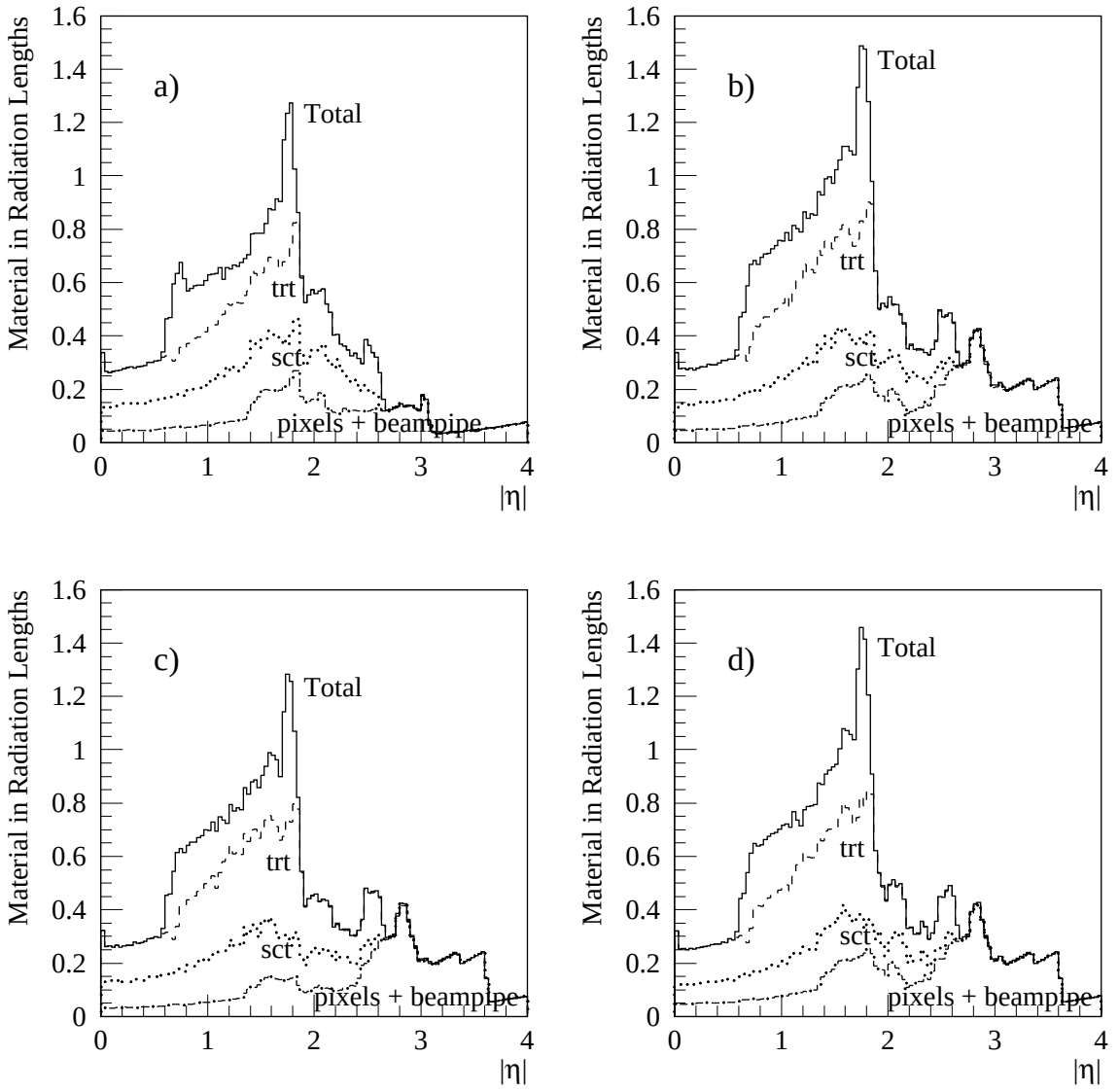

Figure 2-4 Material distribution as a function of η for a) the “TDR” layout, b) the “new TDR” layout, c) the “2+4” layout, d) the “3+3” layout.

Figure 2-4 shows the material distribution, in units of radiation lengths, as a function of η, for the “TDR”, the “new TDR”, the “2+4” and the “3+3” layouts. Figure 2-5 shows the differences in material distributions between the “new TDR” and the “TDR” layouts, and between the “3+4” and the “2+4” and “3+3” layouts, respectively for the pixels and the SCT. Note that in Figures 2-4 and 2-5 the material associated to each detector is only the active material and that part of its own inactive material which is contained within the detector volume, in contrast to Figures 3.18 and 3.19 of the ID TDR, where the material was divided by radial position.

New data sets, consisting of 2500 $H \rightarrow b\bar{b}$ and 10000 $H \rightarrow u\bar{u}$ events, have been generated for each layout. Data sets with high luminosity pile-up (24 minimum bias events for the pixels and SCT and 32 for the TRT) have also been produced for each layout.

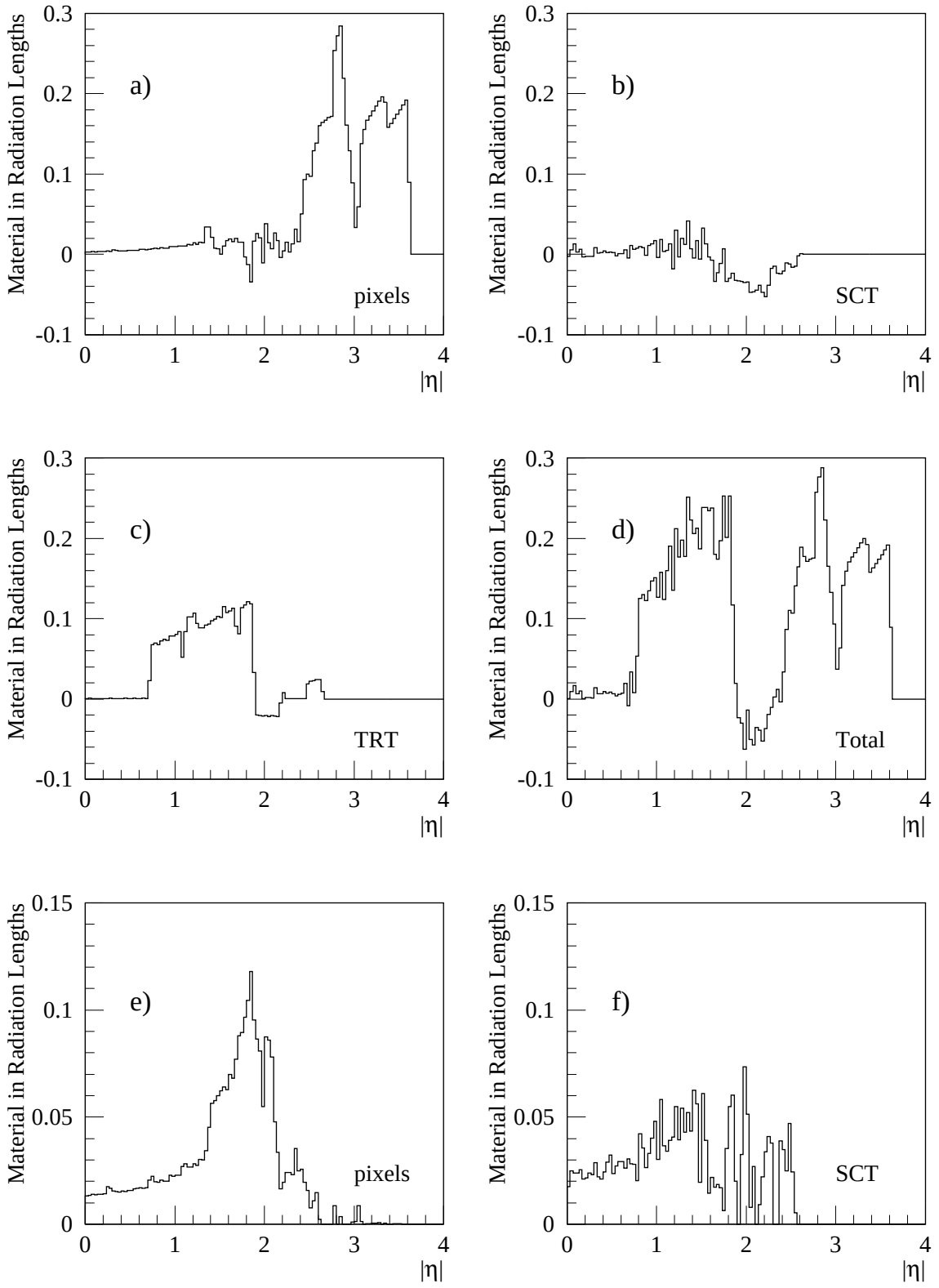

Figure 2-5 a)-d): Differences in material distribution as a function of η between the “new TDR” (“3+4”) and the “TDR” layouts for the pixels (a), the SCT (b), the TRT (c) and the total ID (d). e): Difference in pixel material between the “3+4” and the “2+4” layouts. f): Difference in SCT material between the “3+4” and the “3+3” layouts.

2.3 Pattern Recognition

Although the general philosophy of the pattern recognition programs `xKalman` and `iPatRec` has remained unchanged [3], both of them have undergone significant technical changes. These were necessary to enable the programs to work with equal performance on data sets produced with different geometries, to ignore digits from "suppressed layers" or from "inefficient" detectors, and to work efficiently and in a reasonable amount of time on events with high-luminosity pile-up. In addition, improvements to the performance are continuously being implemented as the understanding of the software progresses.

The program `xKalman` uses a histogramming method to find candidate tracks in the TRT, then extrapolates them into the SCT and pixel detectors using a filtering algorithm (Kalman filter). The track found in the precision detectors is then extrapolated outwards through the TRT to include drift-time hits from the straws which can be unambiguously assigned to each track candidate; finally a global track fit is performed.

The program `iPatRec` uses a combinatorial method to find candidate tracks in the precision detectors, then extrapolates them and associates TRT hits. The final track parameters are also calculated using a global track fit.

3 b-tagging

3.1 Track Selection and Algorithm

The b-tagging performance of different layouts can be compared using as a measure the u-jet rejection at 50% b-tagging efficiency (called R_u in the following). The details of the analysis can be found in the Inner Detector TDR [2]. A brief reminder of the default selection cuts follows:

- jets are defined by collecting all tracks with $p_T > 1$ GeV/c, $|\eta| < 2.5$ and $\Delta R < 0.4$ around the parton directions;
- tracks must satisfy in addition the following quality cuts for b-tagging:
  - at least 9 hits in precision detectors;
  - at least 2 hits in pixel detectors, one of which is in the first pixel layer (B-layer);
  - impact parameter smaller than 1 mm in the R-φ plane;
- the method for b-tagging is a maximum likelihood ratio method based on the significance of the signed impact parameter.

If the cut on the number of precision hits is increased, both the efficiency and R_u are degraded, irrespective of the layout. If, in contrast, this cut is relaxed, the `xKalman` results are not significantly affected, whereas the `iPatRec` results, including R_u, do change significantly.

The b-tagging default cuts are modified in the case of the reduced layouts as follows:

- "2+4": at least 8 hits in precision detectors and 1 hit in pixel detectors;
- "3+3": at least 7 hits in precision detectors and 2 hits in pixel detectors.

3.2 Analysis of the “TDR” Layout with Suppressed Digits

Table 3-1 u-jet rejection for 50% b-jet efficiency (“TDR” layout with suppressed digits).

	xKalman χ^2/dof<3	iPatRec default cuts	iPatRec 7 prec., 2 Pixel hits
3+4*	66±5	66±3	55±2
2*+4	32±1	36±1	48±2
3+3*	62±4	62±3	62±3

A first analysis, using the data sets produced for the ID TDR and the `iPatRec` reconstruction program, has already been published. Ref.[7] contains a detailed description of the procedure and of the performance, if digits from various combinations of detectors are suppressed. Results from `iPatRec` have been presented at the May 1997 ID Performance meeting and results from `xKalman` have also been presented at the September 1997 ID Performance meeting. Here we recall the main results and present in Table 3-1 a comparison of the following analyses:

- reconstruction with `xKalman`, with the addition, for the sake of comparison with `iPatRec`, of a cut on the quality of the track fit: χ^2/dof<3 (this cut is intrinsic in the `iPatRec` pattern recognition procedure);

- reconstruction with `iPatRec` with the default cuts;

- reconstruction with `iPatRec` applying the same cuts for each layout: 7 hits in the precision detectors, including 2 pixel hits (one of which in the B-layer), plus the 1 mm impact parameter cut.

As can be seen from the first two columns of Table 3-1, the two reconstruction programs, although using different algorithms, agree to a good accuracy for all layouts. The errors on the R_u values are strongly correlated, as the same events are used for all analyses. The errors on differences are therefore much smaller than the errors on the absolute values of R_u.

The default cuts give similar track reconstruction efficiencies for the different layouts, accompanied by a significant increase in the number of fakes and secondaries for the reduced layouts. A large degradation is observed for the “2*+4” layout, where the dominant effect is due to tracks with wrongly associated pixel hits. For the “3+3*” layout, the suppressed SCT layer is further away from the vertex region, thus the degradation is less pronounced.

Using the same cuts for all layouts gives similar fake rates in each case and a somewhat smaller increase of the secondary rate for the reduced layouts. The reconstruction efficiency is also higher for the TDR layout. However for the TDR layout there is an increase in the number of secondaries produced after the B-layer with a wrong hit associated in this layer, accounting for the anomalous reduction in rejection observed when comparing the TDR to the “3+3*” layout. In the case of `iPatRec`, these wrongly associated secondaries are characterised by very low track fit probabilities which suggest that a harder cut could be made on the fit χ^2 probability. The improved performance obtained with the “7+2” cut in the “2*+4” case is a consequence of the 2 pixel requirement, which reduces the high rate of wrong associations observed on tracks formed from the B-layer and SCT without intervening hits. The 2 pixel minimum is somewhat optimistic for this layout as demanding hits in both layers leaves no contingency for detector degradation effects (inefficiencies).

3.3 Analysis of the "New TDR" and Reduced Layouts

The results in this section are quoted for each of the 3 layouts, for the so-called "default cuts" (Section 3.1) and for the 3 following conditions:

- default conditions: 97% hit efficiency in precision detectors, no pile-up;

- hit efficiency reduced to 90% in the precision detectors. In addition to the original 3% of digits flagged as "inefficient", `xKalman` removes randomly 7% of the digits and `iPatRec` assigns a 3.5% random inefficiency to read-out chips and a 3.5% random inefficiency to whole detector modules. The requirement on the minimum number of precision hits is reduced by one when applying the default cuts;

- with pile-up corresponding to a luminosity of 10^{34} $cm^{-2}s^{-2}$.

It has been found that if the same cuts are applied to `xKalman` and `iPatRec` internally and externally, then the results are in broad agreement (see for example Table 3-1). Therefore, in some of the studies which follow, results are presented from just one of the programs to provide illustration and avoid repetition.

Figure 3-1 shows the rejection factor R_u as a function of ε_b averaged over $|\eta|<2.5$; Figures 3-2 to 3-6 show the η-dependencies of R_u for ε_b=50%, of the primary track finding efficiency, of the secondary rate and of the fake rate. The results from the `xKalman` program are shown with the default selection cuts. The `iPatRec` results are broadly similar, except:

- a sharper dip in efficiency at η~1.5 for primary track reconstruction (~84% for `iPatRec` and ~87% for `xKalman`);

- a much lower fake rate, 0.05% for `iPatRec` and 0.2% for `xKalman`;

- fewer secondaries (~1.8%) as the pattern recognition is initiated from closer to the vertex, before some of the secondaries have been produced.

Some of these differences are due to the implicit χ^2 cut used inside `iPatRec`.

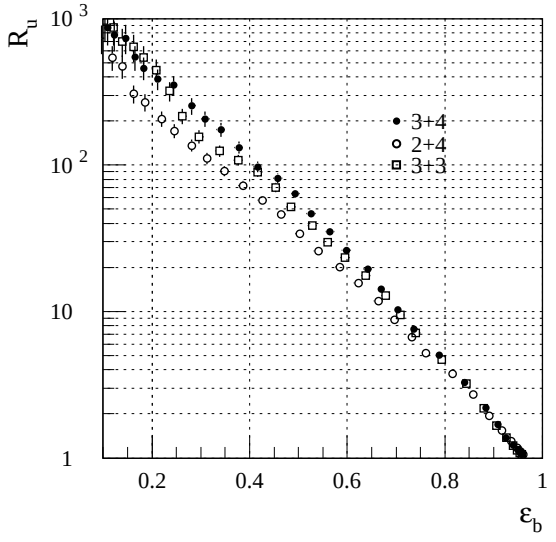

Figure 3-1 u-jet rejection as a function of b-jet efficiency for the default and reduced layouts, with default detector efficiency (xKalman).

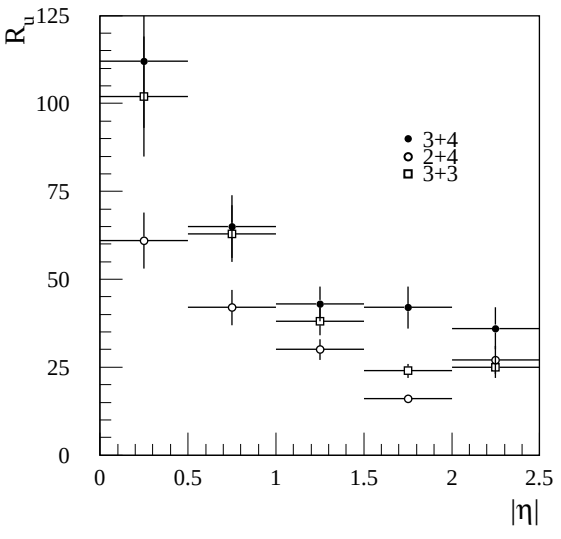

Figure 3-2 u-jet rejection for 50% b-jet efficiency as a function of η for the default and reduced layouts, with default detector efficiency (xKalman).

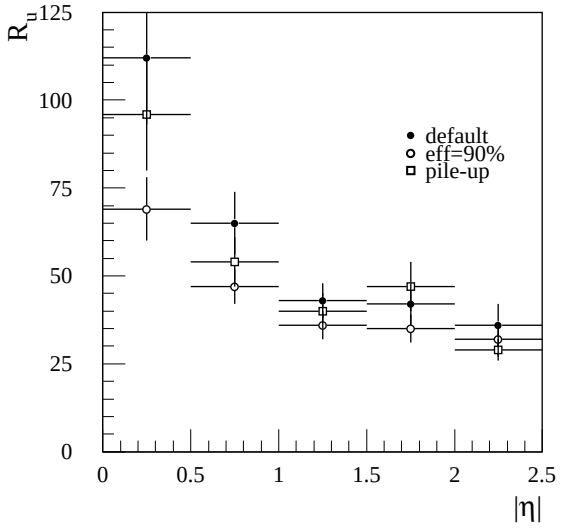

Figure 3-3 u-jet rejection for 50% b-jet efficiency as a function of η for the default layout with default conditions, with 90% detector efficiency and with pile-up (xKalman).

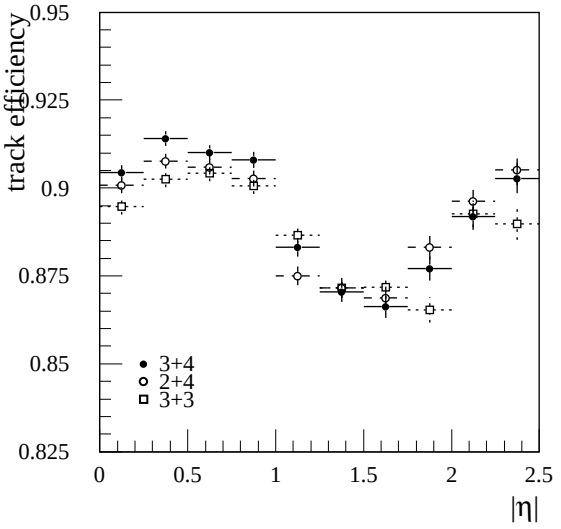

Figure 3-4 Primary track efficiency as a function of η for the default and reduced layouts, with default detector efficiency (xKalman).

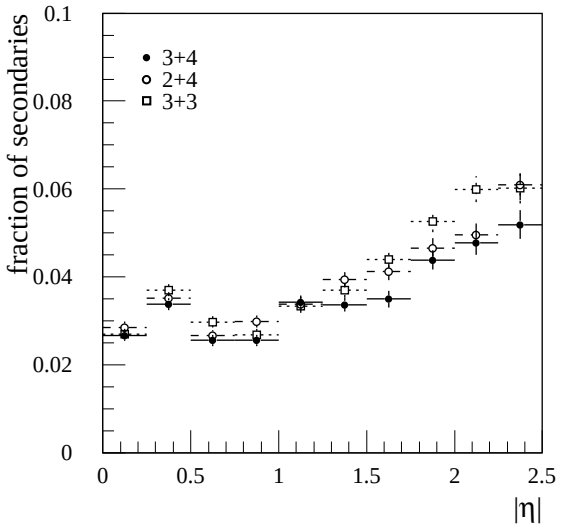

Figure 3-5 Secondary track rate as a function of η for the default and reduced layouts, with default detector efficiency (xKalman).

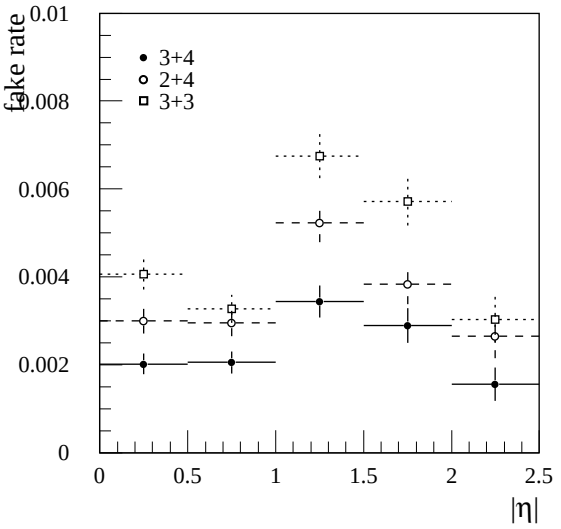

Figure 3-6 Fake track rate as a function of η for the default and reduced layouts, with default detector efficiency (xKalman).

3.3.1 u-jet Rejection

Table 3-2 shows the u-jet rejection for 50% b-jet efficiency found by `xKalman` and `iPatRec` for the default and reduced detector efficiency conditions, and in presence of pile-up (`xKalman` only). A clear degradation is observed for the reduced layouts compared to the default setup. The degradation, over the whole η spectrum, is more pronounced in the case of the "2+4" layout. In the case of "3+3", the degradation happens mainly in the forward region (see Figure 3-2) and is correlated to the increase of secondary tracks (see Figure 3-5).

Table 3-2 u-jet rejection for 50% b-jet efficiency for the default and reduced layouts and for different conditions.

	iPatRec		xKalman		
	default	ε=90%	default	ε=90%	pile-up
3+4	65±4	47±2	60±4	43±2	52±3
2+4	38±2	22±1	35±2	28±1	29±1
3+3	58±3	43±2	47±3	36±2	40±2

Note the decrease in rejection power in the cases of reduced detector efficiency and of pile-up, especially for the reduced layouts. While a 90% detector efficiency could be considered pessimistic, the high-luminosity conditions will certainly occur; it is therefore very important that the detector layout be designed with the high-luminosity performance as reference.

The results for the default conditions are in good agreement with the "suppressed digit" analysis, and give us confidence in the statistical errors. The small difference between the values of R_u found by the two programs can be explained by the presence of the implicit cut on $\chi^2/\mathrm{dof} < 3$ in `iPatRec`.

3.3.2 Track Reconstruction Quality

Table 3-3 Primary track efficiencies, secondary and fake rates in u-jets; rates for ambiguous hit assignments and for non-gaussian tails on primary tracks (xKalman). Typical errors are 0.1% for all rates, except 0.02% for the fake rate.

	default conditions			ε=90%			pile-up		
	3+4	2+4	3+3	3+4	2+4	3+3	3+4	2+4	3+3
primary eff. (%)	89.5	89.3	89.0	83.9	82.9	82.5	87.7	85.8	85.4
secondary rate (%)	3.3	3.6	3.7	3.1	3.4	3.5	3.5	4.6	4.7
fake rate (%)	0.24	0.36	0.46	0.27	0.34	0.51	0.31	0.84	0.86
% tracks with non-unique pixel hits	4.7	8.2	4.9	4.9	8.2	5.1	5.1	8.9	5.3
% tracks with >20% non-unique prec. hits	2.3	5.9	4.6	3.6	6.1	4.8	3.8	8.0	5.8
% tracks in $1/p_T$ tail	1.9	2.3	2.1	2.2	2.9	2.4	2.2	2.5	2.3
% tracks in d_0 tail	1.9	3.2	2.0	2.4	3.7	2.5	2.1	3.5	2.1

The quality of track reconstruction can be estimated by analysing tracks from u-jets. Table 3-3 shows the dependence of the quality of track reconstruction on the layout and the running conditions (detector efficiency and pile-up) obtained with `xKalman`.

Primary tracks are defined as tracks originating less than 2 cm away from the primary vertex. *Secondary* tracks are those produced in secondary interactions in the detector material. These tracks are mainly electrons from photon conversions and most of them have a wrongly associated hit in the B-layer. *Fake* tracks are defined as those having more than 50% of *non-unique* (wrong or shared) hits in the precision detectors.

From the table, it can be seen that the performance is worse for the reduced layouts than the "3+4" layout. In the case of the primary track efficiency, the differences increase when the detector efficiency falls or pile-up is added. In the case of the secondary and fake rates, the differences are affected most strongly by the addition of pile-up. Figures 3-4 to 3-6 show these efficiencies and rates as a function of η for the default conditions.

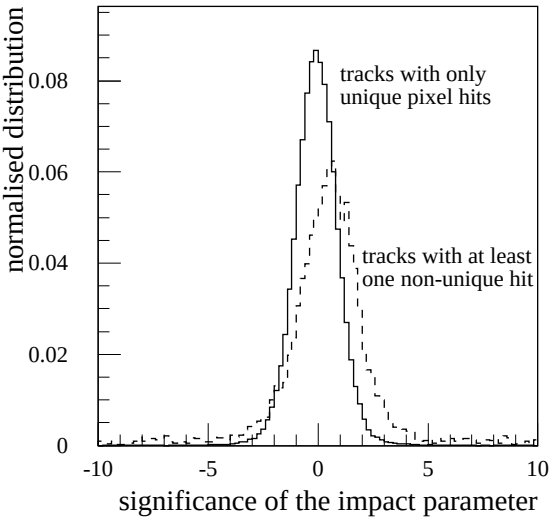

Figure 3-7 Impact parameter significance for primary tracks with only "unique" pixel hits (solid) and with at least a wrong or shared pixel hit (dashed), "3+4" layout (xKalman).

Tracks with more than 20% spoilt (wrong or shared) hits in precision detectors have typically 30% worse p_T resolution and tails beyond 3σ around 10%. Tracks with wrong pixel hits have typically 40% worse impact parameter (d_0) resolution and tails beyond 3σ around 20%. Figure 3-7 shows the impact parameter significance (signed impact parameter divided by its error) for tracks without and with non-unique pixel hits. The distribution is shifted towards positive values as the hit density is higher in the jet core than at the edge of the jet: it is therefore more probable to pick up a wrong hit which pulls the track towards the jet axis. The degradation appears mainly for the "2+4" layout, where the increase in the fraction of primary tracks in the tails of the impact parameter distribution contributes directly to the reduction of the u-jet rejection power.

3.3.3 Further Selection Cuts

The main limitation to the b-tagging performance arises from secondary tracks, i.e. tracks originating from interactions of primary tracks with detector material. In simulated events, one can remove secondary tracks from the list of reconstructed tracks used for b-tagging, using the "truth" information provided by the simulation; in this case, R_u would improve considerably, as shown in Table 3-4. In real events, secondary tracks can only be rejected by applying appropriate cuts on track quality. These cuts have to be adapted to the quality of the tracks being found by the pattern recognition programs, and are therefore different for `xKalman` and `iPatRec`. The additional `xKalman` cuts are:

- impact parameter in the R-z plane relative to the primary interaction point < 1.5 mm;
- χ^2/dof < 3;
- at most 1 shared hit in the pixels;
- at most 2 shared hits in the precision detectors.

Table 3-4 u-jet rejection factors for 50% b-jet efficiency for the default track selection, removing secondary tracks and applying improved cuts.

	iPatRec		xKalman		
	default	ε=90%	default	ε=90%	pile-up
3+4	65±4	47±2	60±4	43±2	52±3
no secondaries			141±14	102±9	106±9
improved cuts	83±6	61±4	81±6	63±4	67±5
2+4	38±2	22±1	35±2	28±1	29±1
no secondaries			54±3	47±3	41±4
improved cuts	58±3	38±2	57±4	47±3	44±2
3+3	58±3	43±2	47±3	36±2	40±2
no secondaries			117±10	75±6	86±7
improved cuts	79±5	51±3	73±5	52±3	59±4

For `iPatRec`, the same cuts are used for all layouts and efficiencies:

- at least 7 hits in precision detectors;

- at least 2 hits in the pixel detectors, one of which is in the B-layer;

- impact parameter smaller than 1 mm in the R-φ plane;

- impact parameter in the R-z plane relative to the intersection of the highest p_T track with the beam axis smaller than 2.0 mm;

- χ^2 probability of the track fit >1%.

The rejection factors calculated with these cuts are also shown in Table 3-4. As an example of the reconstruction performance with these cuts, Figures 3-8 to 3-13 show the rejection factor R_u as a function of ε_b, the η dependence of R_u for ε_b=50%, the primary track finding efficiency, the secondary rate and the fake rate obtained with `iPatRec`.

These improved cuts effectively select a slightly smaller but better measured sample of tracks. The net effect is an increase in R_u for all configurations. Table 3-5 shows the track quality obtained with `iPatRec` before and after applying the improved cuts. Note that what is called the "primary track efficiency" is in fact the fraction of simulated primary tracks which are considered for the b-tagging algorithm; the decrease in this rate is more than compensated by the decrease in secondaries and fakes and the improvement in precision of the measurement of the surviving tracks, as can be seen from the improvement in R_u in most cases.

From Tables 3-4 and 3-5, it is clear that, even with improved track selections, it is not possible to achieve with any of the reduced layouts the same b-tagging performance as with the default layout. This is even more pronounced in the cases of reduced detector efficiency and of high luminosity. Note that the different ways to apply inefficiencies in `xKalman` and `iPatRec` produce slightly different results: in the case of pixel or strip clusters, the random inefficiency applied by `xKalman` will displace the centre of gravity of the remains of the cluster, shifting the reconstructed track from its real trajectory; whereas in the more realistic `iPatRec` scheme, a dead chip (or module) may introduce confusion in the pattern recognition, result in tracks with

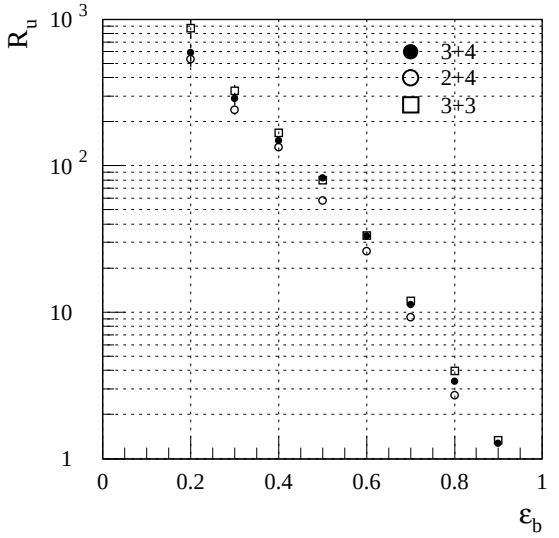

Figure 3-8 u-jet rejection as a function of b-jet efficiency for the default and reduced layouts, with default detector efficiency, after applying improved cuts (iPatRec).

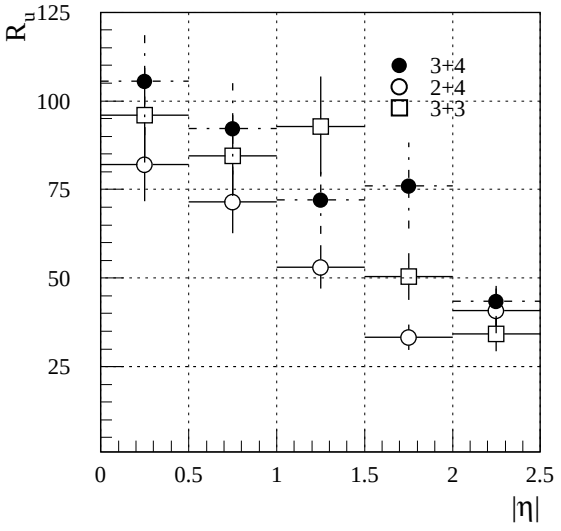

Figure 3-9 u-jet rejection for 50% b-jet efficiency as a function of η for the default and reduced layouts, with default detector efficiency, after applying improved cuts (iPatRec).

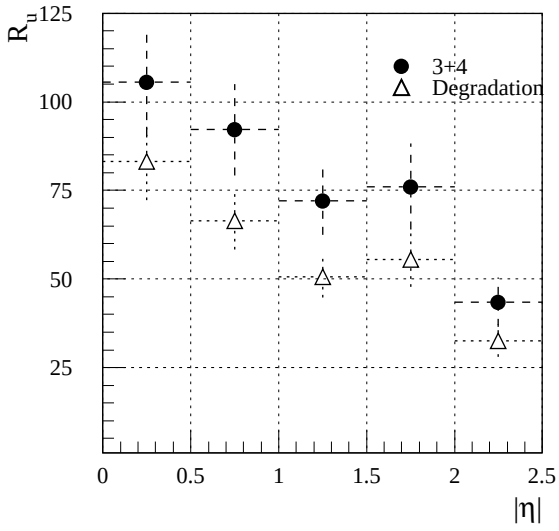

Figure 3-10 u-jet rejection for 50% b-jet efficiency as a function of η for the default layout with default conditions and 90% detector efficiency, after applying improved cuts (iPatRec).

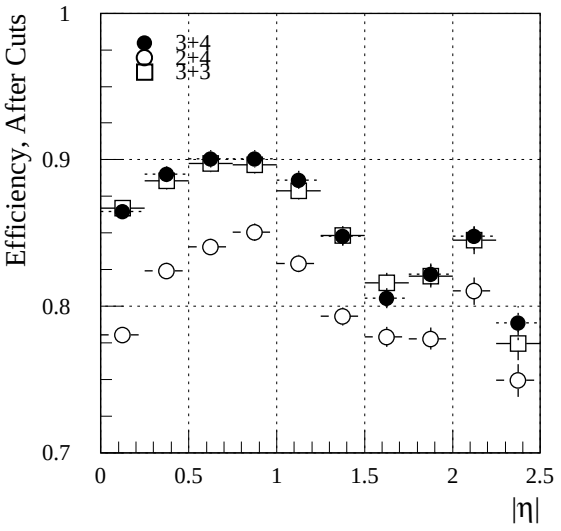

Figure 3-11 Primary track efficiency as a function of η for the default and reduced layouts, with default detector efficiency, after applying improved cuts (iPatRec).

larger errors or lose tracks altogether. The `iPatRec` scheme usually affects several tracks in the same jet and is observed to degrade the b-jet signal more than the u-jet background.

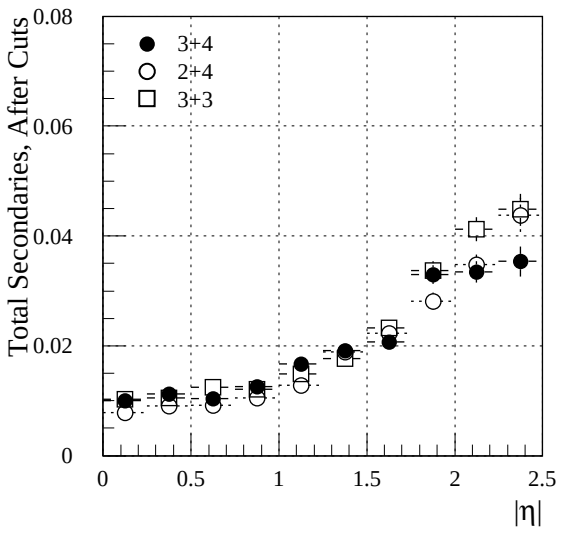

Figure 3-12 Total secondary track rate as a function of η for the default and reduced layouts, with default detector efficiency, after applying improved cuts (iPatRec).

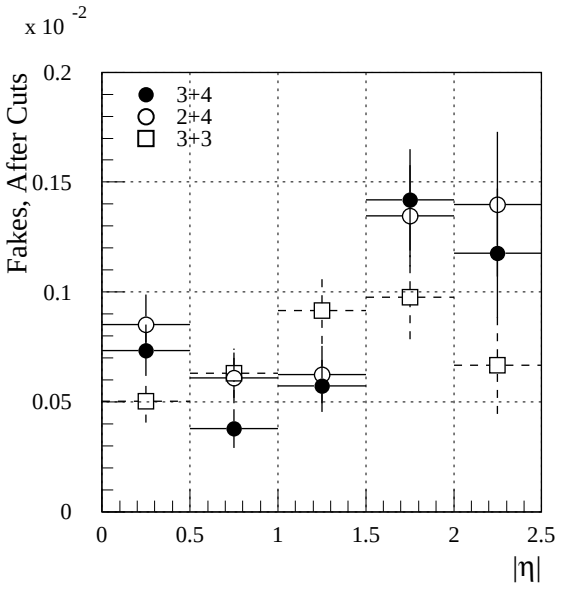

Figure 3-13 Fake track rate as a function of η for the default and reduced layouts, with default detector efficiency, after applying improved cuts (iPatRec).

Table 3-5 Primary track efficiencies, rate of secondaries after the B-layer and fake rate in u-jets, rates for spoilt and wrongly associated hits and non-gaussian tails of primary tracks (iPatRec). The first (second) value is calculated before (after) the “improved cuts”.

	default conditions			ε=90%		
	3+4	2+4	3+3	3+4	2+4	3+3
primary eff. (%)	87.7/86.6	86.9/81.4	89.0/86.3	80.5/79.2	79.7/68.4	78.7/76.1
secondaries after B-layer (%)	0.65/0.40	0.85/0.20	0.72/0.38	0.67/0.39	1.05/0.19	0.67/0.36
fake rate (%)	0.07/0.07	0.17/0.07	0.11/0.07	0.08/0.06	0.25/0.08	0.10/0.06
% tracks with spoilt pixel hits	5.0/4.8	4.5/4.4	5.1/4.8	4.9/4.7	4.6/4.4	5.1/4.7
% tracks with wrong pixel hits	1.8/1.1	4.1/1.5	1.9/1.1	2.0/1.2	6.2/1.7	2.0/1.2
% tracks with spoilt SCT hits	17.0/16.6	15.4/14.9	13.4/13.2	16.0/15.6	14.8/13.9	12.7/12.4
% tracks with wrong SCT hits	1.1/1.1	1.4/1.0	1.0/0.9	1.1/1.0	1.7/1.0	1.0/0.9
% tracks in $1/p_T$ tail	6.4/5.3	6.6/5.1	6.1/5.0	6.4/5.3	7.4/5.1	6.1/5.0
% tracks in d_0 tail	1.8/1.4	3.5/1.8	1.8/1.4	2.0/1.5	5.3/1.9	1.9/1.4

3.3.4 Comparison of u-jet Rejections for m_H=400 and 100 GeV/c^2

All the results quoted above were obtained for jets with an average p_T of 200 GeV/c and an average charged track multiplicity about 10 in a cone with $\Delta R<0.4$ around the b-jet axis. The degradations observed for the reduced layouts are likely to be dependent on track multiplicity and density within jets. In order to estimate this effect, we can compare the results obtained by removing hits (and not layers) for m_H=400 and 100 GeV/c^2 with the "TDR" layout, as shown in Table 3-6. These results are strongly correlated as they are obtained from the same data sets, therefore differences are much more significant than the statistical errors would indicate.

Table 3-6 u-jet rejection for 50% b-jet efficiency with the "TDR" layout, for m_H=100 and 400 GeV/c^2 (xKalman).

layout	m_H = 400 GeV/c^2		m_H = 100 GeV/c^2	
	default cuts	improved cuts	default cuts	improved cuts
3+4*	58±4	82±6	89±7	111±11
2*+4	31±1	52±3	55±4	88±7
3+3*	51±3	74±5	82±7	101±10

As expected, the significantly lower p_T range of the jets from $H \rightarrow b\bar{b}$ decays with m_H = 100 GeV/c^2 results in a significant improvement in R_u with respect to m_H = 400 GeV/c^2. This improvement is seen both in the case of the default cuts and of the improved cuts.

3.4 Implications for Physics

3.4.1 Observation of the Higgs in WH Production

In the ID TDR, the physics potential for observing the Higgs in WH production with m_H = 100 GeV/c^2, $W \rightarrow l\nu$ and $H \rightarrow b\bar{b}$ was studied in some detail [8]. The electron or muon from the W provides the trigger, while the signal is observed in the $b\bar{b}$ invariant mass. The significance of the signal was evaluated in the light of several backgrounds, some of which were reducible (containing non-b jets) and some of which were irreducible (containing b-jets). The raw efficiencies obtained from the ID studies reported earlier in the TDR were transformed into quantities better suited to the parton-labelling in ATLFAST[1] and the efficiencies were evaluated as functions of the jet p_T.

The table of [8] explicitly identifies all jet types in terms of b, c or light-quark (or gluon) jets, and the contribution of each process to the total rate in the mass interval is directly proportional to the product of the efficiencies for selecting each jet type as a b-jet. Hence the different contributions can readily be evaluated for different values of the efficiencies. This has been done with the following assumptions:

1. For example, what was generated as a u-jet in the ID study may have undergone significant hard gluon emission followed by gluon splitting to a $b\bar{b}$ pair which would be labelled as a b-jet in ATLFAST.

- b-jet efficiencies for vertex tagging are taken as 50%[1], and the rejections against other jets are evaluated at this efficiency. The efficiency for the inclusion of a soft-lepton tag is assumed unchanged.
- c-jet efficiencies are assumed unchanged at 15%.
- light-quark efficiencies needed as input to the calculations of [8] can be derived by scaling by the ratio of the appropriate rejection obtained in the earlier sections of the TDR (50 in the case of m_H = 400 GeV/c^2 and 80 in the case of m_H = 100 GeV/c^2) and the values of R_u found in this work.[2]

The calculations contained in the TDR correspond to m_H = 100 GeV/c^2 and an integrated luminosity of 3×10^4 pb^{-1}, while the majority of studies described in this note correspond to m_H = 400 GeV/c^2. The last assumption listed above allows for the p_T dependence of the rejection (as illustrated in Figure 6-59 of the TDR) in a simple way – it is impossible to do better without repeating the ATLFAST simulations which were performed for the TDR. However, the assumption is likely to cause overestimation of the consequences of reduced layouts for the 100 GeV/c^2 Higgs, since the more energetic jets will be tighter and hence more prone to confusion.

In what follows, two quantities have been examined:

- The significance (S) of the signal, defined as $signal/\sqrt{background}$.
- The ratio (R_{bgnd})[3] of the *reducible* to *irreducible* backgrounds. The most important reducible backgrounds arise from QCD processes with relatively large and theoretically uncertain cross-sections, such as Wjj. The rate for these events is reduced substantially by large rejection factors R_u for the light-quark jets. Consequently, the rate of these backgrounds is very uncertain, owing to the large to uncertainties in the cross-section and the tagging. Hence, the larger R_{bgnd}, the greater the potential for large systematic errors in the estimation of the significance of a Higgs signal.

Figure 3-14 shows the significance which can be obtained as a function of R_u, where R_u corresponds to the values evaluated for m_H = 400 GeV/c^2. It can be seen that, for R_u greater than ~50, the significance changes quite slowly since the backgrounds with heavy-flavour jets dominate. Figure 3-15 shows the ratio of reducible to irreducible backgrounds. This does not fall to zero as R_u becomes large because of the presence of backgrounds containing charm. The fractional changes in this ratio do not depend strongly on the use of the lepton tag, and for what follows only the ratios for the vertex tag alone are given. As in the case of other physics channels, it is desirable to achieve R_{bgnd} values well below one for the reasons mentioned above.

Tables 3-7 and 3-8 show the expectations using the values of R_u corresponding to xKalman with the "improved cuts" taken from Table 3-4 (for m_H = 400 GeV/c^2) and Table 3-6 (for m_H = 100 GeV/c^2 and with the original "TDR" layout). The fractional changes relative to the "3+4" layout are shown for the different quantities. The sensitivity to the layout changes is reduced compared to previous presentations [9] because of the "improved cuts". These cuts have reduced the differences in R_u between the various layouts (see Table 3-4). Also, since the values

1. This manifests itself as 53% in the TDR, since some allowance was made for selection cuts in the analysis.
2. For example, a value of R_u = 81 for m_H = 400 GeV/c^2 would lead to the light quark jet efficiency being multiplied by 50/81.
3. This quantity was called $R_{red/irred}$ in the Inner Detector TDR.

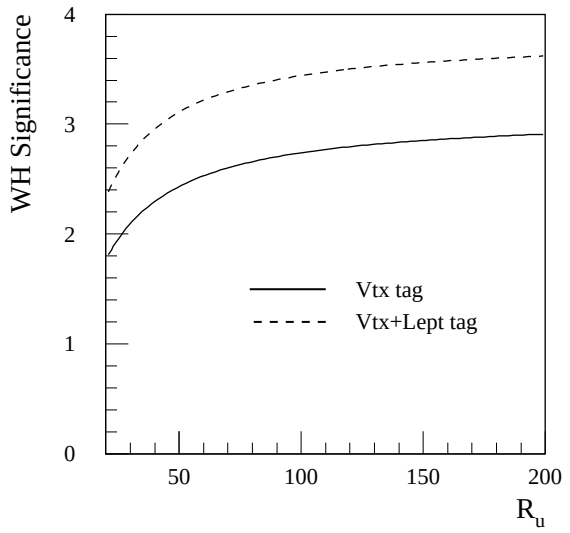

Figure 3-14 Significance for WH signal as a function of R_u (R_u evaluated for m_H = 400 GeV/c^2), for an integrated luminosity of 3x10^4 pb^{-1}.

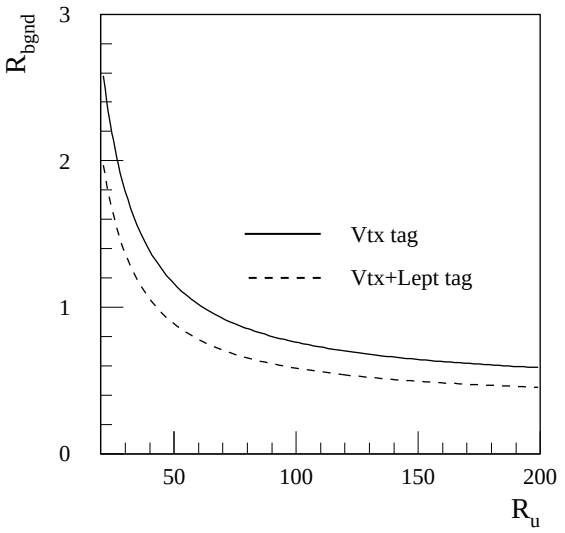

Figure 3-15 Ratio of reducible to irreducible backgrounds R_{bgnd} as a function of R_u (R_u evaluated for m_H = 400 GeV/c^2).

of R_u have been increased by the cuts, the reducible background has become less important relative to the irreducible background – the values of R_u are in a place on the significance curves of Figure 3-14 with a smaller gradient. Hence it is very important to consider what happens with reduced values of R_u where the gradient of the significance distribution is greater. This is the case for the examples of reduced detector efficiency and pile-up – information which is only available for m_H = 400 GeV/c^2 data. Note the considerable reduction in significance with respect to the default conditions.

Using the rejections obtained for m_H = 400 GeV/c^2, it can be seen that if a pixel layer is removed, the significance of a WH signal will be reduced by ~6%; if an SCT layer is removed, this

Table 3-7 Changes resulting from various layouts in the significance (S) for a WH signal with m_H=100 Gev/c^2 (without and including a soft-lepton tag) and in the ratio of reducible to irreducible backgrounds (R_{bgnd}), for an integrated luminosity of 3x10^4 pb^{-1}.

	Using R_u with m_H = 400 GeV/c^2			Using R_u with m_H = 100 GeV/c^2 (original TDR Layout; digits suppressed)		
	3+4	2+4	3+3	3+4*	2*+4	3+3*
R_u	81	57	73	111	88	101
ΔR_u (%)	–	–30	–10	–	–21	–9
S	2.66	2.50	2.62	2.60	2.49	2.55
ΔS (%)	–	–6.0	–1.6	–	–4.4	–1.7
S_{+lept}	3.36	3.19	3.32	3.29	3.17	3.24
ΔS_{+lept} (%)	–	–5.2	–1.4	–	–3.8	–1.4
R_{bgnd}	0.85	1.06	0.90	0.93	1.08	0.99
ΔR_{bgnd} (%)	–	+24	+6	–	+17	+6

Table 3-8 Changes resulting from various layouts in the significance (S) for a WH signal with m_H=100 Gev/c^2 (without and including a soft-lepton tag) and in the ratio of reducible to irreducible backgrounds (R_{bgnd}), for an integrated luminosity of 3x10^4 pb^{-1} – showing the effect of reduced detector efficiency and pile-up.

	Using R_u with m_H = 400 GeV/c^2 ε = 90%			Using R_u with m_H = 400 GeV/c^2 with pile-up		
	3+4	2+4	3+3	3+4	2+4	3+3
R_u	63	47	52	67	44	59
ΔR_u (%)	–	–25	–17	–	–34	–12
S	2.55	2.40	2.45	2.58	2.36	2.52
ΔS (%)	–	–6.1	–3.9	–	–8.7	–2.4
S_{+lept}	3.24	3.07	3.13	3.27	3.03	3.21
ΔS_{+lept} (%)	–	–5.3	–3.4	–	–7.6	–2.0
R_{bgnd}	0.99	1.22	1.13	0.95	1.28	1.03
ΔR_{bgnd} (%)	–	+23	+14	–	+35	+9

reduction would be ~2%. As expected, the sensitivity to the reductions in layout is smaller for m_H = 100 GeV/c^2, giving ~4% and ~1.5% respectively.

Figure 3-16 shows how the significance of a WH signal varies with the choice of efficiency for tagging b-jets. To calculate this information, R_u and R_c have been taken as functions of ε_b: R_u is taken from curves similar to Figure 3-1, but with the "improved cuts"; the behaviour of R_c is strongly related to the cuts on the jet significance (see Section 3.1) rather than the performance of the pattern recognition and has been extracted from Figure 6-49 of the TDR. There are small errors on the points arising from statistical errors in the original simulations and in determining the data from various graphs. The curves justify the choice of the 50% point as a good working point (significance is maximal and insensitive to choice of ε_b) in agreement with [10] and give the greatest sensitivity to different layouts.

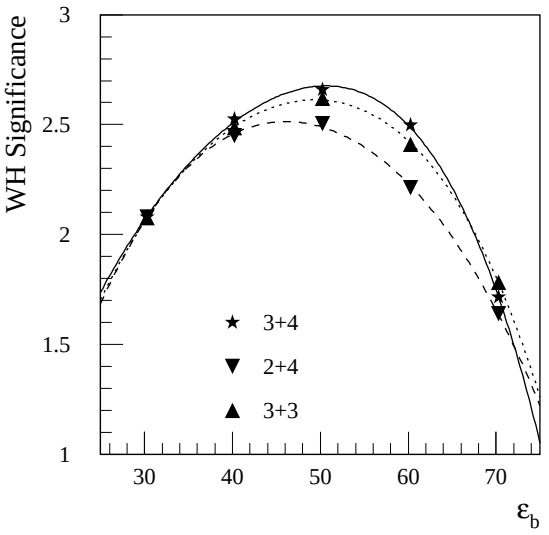

Figure 3-16 Significance of the WH signal with m_H=100 Gev/c^2 as a function of ε_b, corresponding to R_u evaluated for m_H=400 GeV/c^2 with "improved cuts", for an integrated luminosity of 3x10^4 pb^{-1}.

3.4.2 Other Physics Using b-tagging

3.4.2.1 Top Physics

b-tagging will be an essential component in Top Physics – see Section 11.10 of the Technical Proposal [11]. For Top Physics itself, the b-tagging is not quite so crucial since there is a huge cross-section for $t\bar{t}$ production (6×10^4 pairs per day at 10^{33} $cm^{-2}s^{-1}$) and, with this rate, there is the possibility of demanding very clear signatures, e.g. including both an electron and a muon from the two W's, or requiring top quarks with very high p_T. On the other hand, as shown in [12], the complete reconstruction of $t\bar{t}$ pairs with purely hadronic decays from the top quarks is subject to large combinatorial backgrounds from other jets in the events, and therefore b-tagging turns out to be a powerful tool to minimise this type of background.

3.4.2.2 Observation of the Higgs in $t\bar{t}H$ Production

The sensitivity to $H\rightarrow b\bar{b}$ in WH production shown above is marginal. This signal will be complemented by $t\bar{t}H$ production, where a search is made for 3 or 4 b-jets [10]. The previous studies showed that the greatest sensitivity came from demanding only 3 b-jets. However, there are significant combinatorial backgrounds arising in the signal events from the 3 different pairings of the candidate b-jets to form the Higgs; further, the signal and background shapes are very similar. Therefore, it is felt necessary to demand 4 b-jets and to consider complete reconstruction of both top quarks [13].

It is less easy to estimate the sensitivity to R_u for $t\bar{t}H$ production since the different components of the background (specifically, the flavour of QCD jets) are not explicitly given in [10]. To provide some quantitative estimate of the sensitivity of this analysis to R_u, the information in Table 19 of [10] for 4 b-jets has been considered and simple assumptions as to the nature of the irreducible backgrounds have been made. After 3 years of low luminosity running (3×10^4 pb^{-1}), with ε_b=50% and R_u=80, a sensitivity of 1.9 could be achieved. The most important source of background is the process $t\bar{t}jj$, where the reducible and irreducible components are of the same magnitude. A 10% (30%) reduction in R_u would reduce the sensitivity by about 2% (9%). While this channel is more difficult to reconstruct completely than the WH channel, it will be easier to search for at high luminosity, due to the absence of the tight jet veto cuts applied to the WH candidate events in order to reduce the large backgrounds.

3.4.2.3 SUSY Spectroscopy

Precisely which SUSY particles and decays are observable will depend significantly on the model parameters. Nevertheless, it is clear that b-tagging will play a significant role [14], especially for the so-called Points 1, 2 and 5 where $\chi^0_2\rightarrow h\chi^0_1$ with $h\rightarrow b\bar{b}$ (χ^0_1 is the LSP) is kinematically allowed.

The light SUSY Higgs h should be copiously produced at low luminosity and its mass determined from the $b\bar{b}$ invariant mass. The other neutral Higgs A and H, might be observable after high luminosity running through $b\bar{b}A,H$ production with $A,H\rightarrow b\bar{b}$ [15]. In this case also, b-tagging will be of great importance since four b-jets have to be identified in each event (as in the case of $t\bar{t}H$ production).

The reconstruction of $h\rightarrow b\bar{b}$ will often be the starting point for SUSY spectroscopy:

- the gluino can be reconstructed through the decay: $\tilde{g} \rightarrow bb$ with $b \rightarrow b\chi^0_2$, $\chi^0_2 \rightarrow h\chi^0_1$ and $h \rightarrow b\bar{b}$ – giving a 4 b-jet final state;
- the squarks can be reconstructed through the decay: $\tilde{q}_L \rightarrow q\chi^0_2 \rightarrow qb\bar{b}\chi^0_1$ – the $\tilde{q}_L$ mass being determined from the end-point in the $qb\bar{b}$ mass spectrum.

While the h mass can be determined well with modest b-tagging capability, it is essential to have good performance to ensure that the signal to background ratios are well controlled to permit the careful determination of the complete mass spectrum of SUSY particles. To keep the ratio (S/B) of fake b's to real b's to less than 10% when looking for inclusive signatures containing $h \rightarrow b\bar{b}$, R_u must be > 50. The recommendation presented at the SUSY workshop [16] was that ATLAS needs $\varepsilon_b = 60\%$, $R_u = 100$ (with $R_c = 10$), leading to S/B = 1.8 for the $h \rightarrow b\bar{b}$ signal above the combinatorial SUSY background. The results presented in this note show that the reduced layouts would lead to a highly undesirable loss of performance for this crucial physics.

4 Other Consequences for the Inner Detector

4.1 Level-2 Rates for Electron Triggers

The ID provides two independent Level-2 triggers: one from the precision layers and a second from the TRT. It is anticipated that these will be ANDed to reduce the rate. Clearly if the number of precision layers is reduced, the performance of the corresponding trigger will be degraded. Preliminary studies have been made at 10^{34} $cm^{-2}s^{-1}$ of electrons of $E_T = 30$ GeV and of backgrounds coming from jets. As in the ID TDR (Section 7.3), Level-2 calorimeter cuts have been applied and matching to the Level-2 Ecal cluster is required. Figures 4-1 and 4-2 show the efficiencies and rates for the precision layers alone and the combination with the TRT. This is shown for the original TDR layout, with various layers suppressed as required, i.e. 3+4*, 3+3*, 2*+4 and 2*+3*.

It is not easy to make comparisons between different layouts, due to the discrete nature of the cuts on the number of hits on tracks. Nevertheless, several conclusions can be drawn:

- The results of removing a pixel or an SCT layer are similar.
- For the trigger using the precision layers alone, if one layer is removed, and if one reduces the requirement on the number of precision space-points from ≥4 to ≥3, the efficiency for electrons can be maintained at the cost of a ~40% increase in rate. The uncertainty on this expected increase is of course very large.
- This degradation of the Level-2 trigger performance is avoided if the TRT is included.
- If both a pixel and an SCT layer are removed, then without or with the TRT, the efficiency cannot be maintained and falls by ~3% to 92.5% or 88% respectively, if the background rate remains the same.

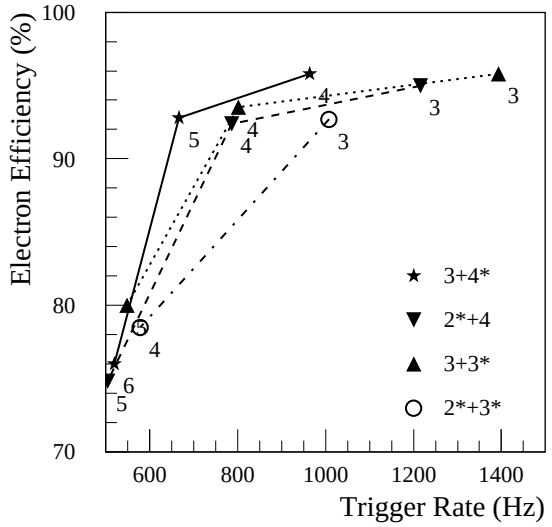

Figure 4-1 Efficiencies for electrons of E_T = 30 GeV as a function of Level-2 trigger rate, using the Ecal and the precision layers.

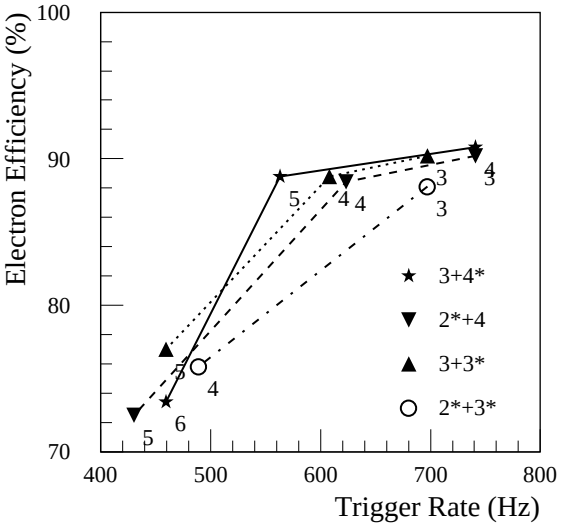

Figure 4-2 Efficiencies for electrons of E_T = 30 GeV as a function of Level-2 trigger rate, using the Ecal, the precision layers and the TRT.

4.2 K^0_s Reconstruction

The SCT layers are important for reconstructing $K^0_s \to \pi^+\pi^-$ decays, for example in $B^0_d \to J/\psi + K^0_s$ decays. The mean energy of K^0_s's from B^0_d decays is 5.4 GeV, resulting in a $\gamma c\tau$ value of 29 cm. The analysis reported in Section 6.5 of the ID TDR demanded 4 hits per track in at least 2 super-layers – the minimum required to fully reconstruct the momentum vector of a K^0_s. The efficiency for reconstructing K^0_s decays as a function of decay radius is shown in Figure 4-3. Should one set of SCT layers be removed, then it is anticipated that the layers in the barrel would be evenly spaced (as described in Section 2.2), causing the 2nd from last layer to be moved inwards by 3.7 cm. This would result in a reconstruction efficiency loss of at least 5% for K^0_s decays; this loss would obviously increase in case of a reduced detector efficiency.

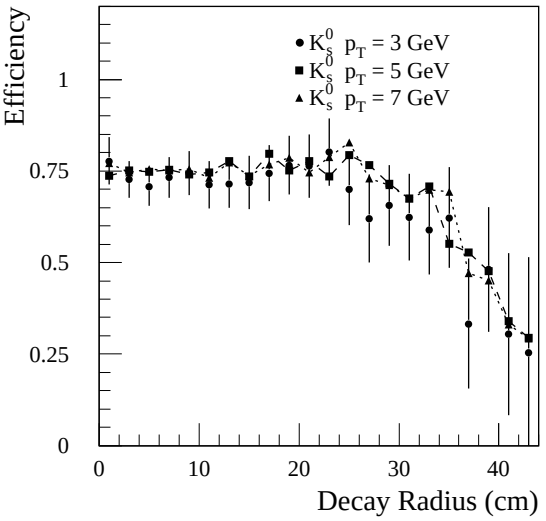

Figure 4-3 K^0_s efficiency as a function of radius for TDR layout.

5 Calorimeter Performance

The main effect of the Inner Detector material on the electromagnetic calorimeter performance is to produce low-energy tails in the calorimeter energy measurement. A photon/electron shower which starts in the Inner Detector is opened in φ by the magnetic field, the effect being larger for the smaller particle energies and interaction radii. In order to preserve the shower containment in the EM calorimeter, and therefore a good energy resolution, a large and asymmetric cluster (bigger in φ than in η) has to be used. For instance, whilst for unconverted photons clusters of size 3×5 cells in Δη×Δφ are large enough to contain the shower, low-energy electrons (E < 100 GeV) and converted photons[1] have to be reconstructed in clusters of 3×7 cells in Δη×Δφ. Despite this, low-energy tails persist, as shown in Figure 5-1. The use of clusters larger than 3×7 cells is prevented by the fact that the contribution of the electronic and pile-up noise to the energy resolution would become intolerably large [17]. Figure 5-1 also shows that the tails are larger for small interaction radii, therefore the material in the innermost layers of the Inner Detector is potentially the most damaging for the calorimeter performance.

The impact of the three Inner Detector layouts discussed in the previous sections on the EM calorimeter performance has been determined by looking at the calorimeter response to single electrons and by evaluating the experimental acceptance for the two most sensitive physics channels: $H \rightarrow \gamma\gamma$ and $H \rightarrow ZZ^* \rightarrow 4e$.

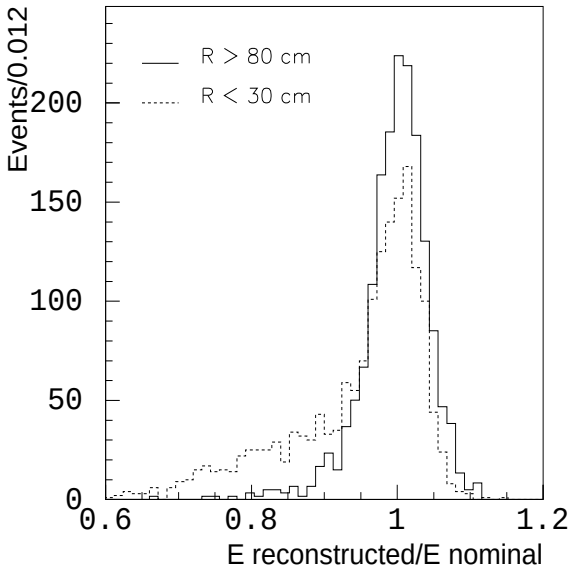

Figure 5-1 Energy spectra reconstructed in the EM calorimeter in a $\Delta\eta \times \Delta\varphi = 3 \times 7$ cell cluster (normalised to the generated particle energy), for electrons of E_T = 10 GeV at η = 1.2. The full (resp. dashed) histogram is for electrons with an interaction radius larger than 80 cm (resp. smaller than 30 cm).

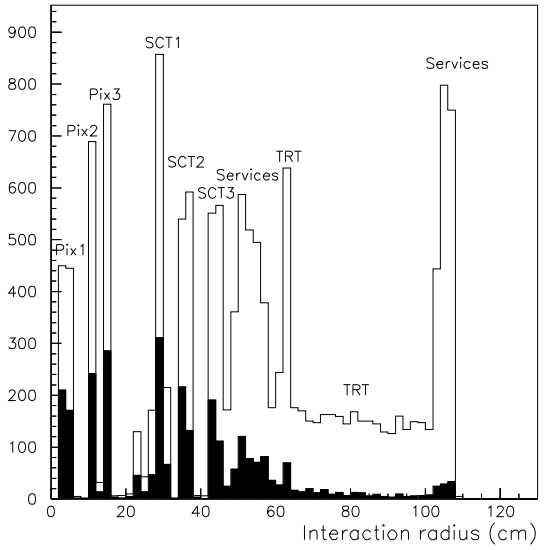

Figure 5-2 Distribution of the interaction radius, defined as the radius at which the electron has emitted the hardest Bremsstrahlung photon, for electrons of E_T=10 GeV at η=1.2. The white histogram is for all electrons whilst the black histogram is for electrons in the low-energy tails of the calorimeter energy measurement.

1. Throughout this note, a photon is considered as converted if the conversion occurs at a radius smaller than 80 cm and a z-position smaller than 280 cm, i.e. in the region where it can be efficiently identified by the Inner Detector.

5.1 Tails in Electron p_T Distributions

Low-energy tails and their dependence on the interaction radius have been studied with electrons of E_T=10 GeV at η=1.2. At this rapidity, the material in the Inner Detector reaches 0.8 X_0 (see Figure 2-4) and low-E_T electrons are affected the most by it. Figure 5-2 shows the distribution of the interaction radius, defined as the radius at which the electron has radiated the hardest Bremsstrahlung photon, for the "3+4" layout. Clear peaks are visible at the positions of the Pixel and Silicon layers[1], as well as a continuous distribution in the TRT region. The open histogram is for all electrons and the shape and height of the peaks simply reflect the distribution and amount of material in the various parts of the Inner Detector. The black histogram is for electrons in the low-energy tails of the calorimeter energy measurement, i.e. below -2.5σ from the peak of the energy distribution (σ=3.5% is the calorimeter energy resolution without the contribution of the electronic and pile-up noise). At this rapidity, the fraction of events in the tails is 19.2±0.6%. It can be seen that the tails are populated mainly by electrons, which have interacted in the precision layers of the Inner Detector. A more quantitative estimate of the contribution of the various layers to the tails is given in Table 5-1. Each of the pixel and SCT layers produces about 2% of tails. A similar contribution comes from the ensemble of the TRT and the services running at the external radius, despite the fact that the total material in this region is much larger than in a single precision layer. Some decrease of the tails with radius is visible also in the three SCT layers. The typical error on these numbers is 0.2%. Table 5-1 shows also the total amount of tails and their breakdown for the reduced layouts. In both cases, the total fraction of events in the tails is about 16%, which represents a gain of 15% with respect to the baseline layout.

Table 5-1 Contributions to the calorimeter low-energy tails coming from the various concentrations of material of the Inner Detector for the three considered layouts. The units are % of the total number of electrons and the errors are ~0.2%.

	3+4	2+4	3+3
Beam pipe	0.5	0.5	0.4
Pixel B-layer	2.2	2.2	2.2
Pixel barrel 1	2.3	–	2.1
Pixel barrel 2	2.2	2.1	2.0
Pixel support	0.4	0.3	0.3
SCT barrel 1	2.5	2.4	2.2
SCT barrel 2	2.2	2.2	1.7
SCT barrel 3	1.9	1.5	–
SCT services	2.4	2.5	2.3
TRT total	2.4	2.4	2.3
TOTAL	19.2±0.6	16.1±0.6	15.6±0.5

1. Note that at this rapidity, the electron track crosses only three SCT layers before entering the end-cap region.

5.2 Consequences for H $\rightarrow \gamma\gamma$

Table 5-2 Main results for the H $\rightarrow \gamma\gamma$ channel (m_H=100 GeV/c^2) obtained with the three layouts. The statistical error on the acceptances and efficiencies is 0.5%.

	3+4	2+4	3+3
Events with converted γ	39.6%	35.8%	35.6%
Photon efficiency	78.1%	79.9%	78.2%
Acceptance in mass bin (unconverted photons)	84.2%	83.7%	84.0%
Acceptance in mass bin (all photons)	80.0%	80.8%	80.0%
Relative $S/\sqrt{B}$	1	1.03	1.00

The impact of the Inner Detector layout on the H $\rightarrow \gamma\gamma$ channel has been studied for m_H=100 GeV/c^2. About 10000 events were fully simulated in the ATLAS detector for the three layouts. The statistics is reduced to about 4000 events per layout after the kinematic and photon identification cuts. Table 5-2 summarises the main results obtained with the three layouts. The fraction of events containing at least one converted photon decreases from about 40% in the "3+4" layout to about 36% in the reduced layouts. The photon identification efficiency is 2% larger in the "2+4" layout than in the two other layouts, owing to the reduced amount of material at small radius. The acceptance for unconverted photons in the optimum mass bin of $\pm 1.4\sigma$ (σ=1.3 GeV/c^2 is the mass resolution including all contributions) is about 84%, and is the same for the three layouts, as expected. When all photons are considered, the acceptance in the mass bin is 1% larger for the "2+4" layout, again owing to the reduced amount of material at small radius. Note that the acceptance in the mass bin for a gaussian distribution would be 83.8%, so the tails are at the level of 4%. The last row of Table 5-2 shows that the "2+4" layout would provide a gain of 3% in the signal significance at high luminosity with respect to the "3+4" layout. Part of this gain would come from the larger photon identification efficiency and part from the larger acceptance in the mass bin. On the other hand, the "3+3" layout would not provide any significant gain with respect to the "3+4" layout for the H $\rightarrow \gamma\gamma$ channel.

5.3 Consequences for H $\rightarrow ZZ^* \rightarrow$ eeee

The H $\rightarrow ZZ^* \rightarrow$ 4e channel is expected to be more sensitive than the H $\rightarrow \gamma\gamma$ channel to the amount of material in the Inner Detector, because of the presence of four electrons of relatively low p_T in the final state. About 4000 H $\rightarrow ZZ^* \rightarrow$ 4e events with m_H=130 GeV/c^2 have been fully simulated in the ATLAS detector for each layout. About 1500 events per layout survive the kinematic cuts. Table 5-3 shows the resulting acceptances for the three layouts in the optimum mass bin of $\pm 2\sigma$, where σ=1.4 GeV/c^2 is the mass resolution including only the sampling term (no noise, no pile-up, no constant term). Results obtained with internal Bremsstrahlung switched off and on are shown separately. With the "3+3" layout, the acceptance in the mass bin would increase by about 2% with respect to the "3+4" layout. With the "2+4" layout, the acceptance would increase by 3-4%. This translates into a maximum gain of 2% (3-4%) in the signal significance for the "3+3" layout ("2+4" layout) with respect to the "3+4" layout.

Table 5-3 Acceptance in the optimum mass bin (±2σ) for the $H \rightarrow ZZ^* \rightarrow 4e$ channel with m_H=130 GeV/c^2 for the three layouts. Results are shown separately for events with internal Bremsstrahlung switched on and off.

	3+4	2+4	3+3
Acceptance in mass bin (Internal Bremsstrahlung off)	86.2±1.5%	89.0±1.6%	88.3±2.0%
Acceptance in mass bin (Internal Bremsstrahlung on)	81.0±1.5%	85.1±1.5%	82.6±2.0%

5.4 Conclusion on the EM Calorimeter Performance

The impact of the reduced layouts on the EM calorimeter performance is small but visible, and can be summarised as follows. The low-energy tails for electrons of E_T=10 GeV at η=1.2 decrease by about 15%. The "2+4" layout would provide a gain of 3% in the significance of the $H \rightarrow \gamma\gamma$ channel and of up to 4% in the significance of the $H \rightarrow ZZ^* \rightarrow 4e$ channel. The "3+3" layout would provide no improvement for the $H \rightarrow \gamma\gamma$ channel, but would provide a gain of up to 2% in the significance of the $H \rightarrow ZZ^* \rightarrow 4e$ channel.

6 Conclusions

In conclusion, it has been shown that both reduced layouts, while giving a slightly better EM calorimeter performance, give a significantly degraded Inner Detector performance compared to the baseline layout, for b-tagging (including Higgs searches, top and SUSY physics), Level-2 triggering and K^0_s reconstruction. In particular, the significance of the WH channel, already marginal, is reduced even further. As shown here, there will be serious degradations in the ID performance arising from the inevitable effects of reduced detector efficiency and pile-up. The Inner Detector Community believes that it is highly undesirable to incur additional and avoidable degradations arising from a reduced layout. The impact on the calorimeter performance is being addressed by seeking reductions in passive material, rather than in sensitive elements. The layout with 7 precision layers will give the best overall performance for ATLAS; it is therefore recommended to keep it as the baseline layout.

Acknowledgements

We would like to thank Daniel Froidevaux and Tony Weidberg for some valuable discussions and for their encouragement.

References

1 ATLAS Collaboration, Calorimeter Performance Technical Design Report, CERN/LHCC/96-40 (ATLAS TDR 1), Section 2.3.1

2 ATLAS Collaboration, Inner Detector Technical Design Report, Volume I, CERN/LHCC/97-16 (ATLAS TDR 4), Section 6.7

3 ATLAS Collaboration, ID TDR, Section 2.5.2

4 ATLAS Collaboration, ID TDR, Chapter 3

5 ATLAS Collaboration, ID TDR, Section 3.1.5

6 A. Rozanov, http://marpix1.in2p3.fr/Pixel/dice/twothree/material.ps

7 A. Poppleton and G. Stavropoulos, ATLAS Internal Note InDet-No-152, June 1997

8 ATLAS Collaboration, ID TDR, Section 6.7.8

9 A. Parker, presentation at the plenary meeting, September 1997 ATLAS week

10 D. Froidevaux and E. Richter-Was, ATLAS Internal Note Phys-No-043, September 1994

11 ATLAS Collaboration, Technical Proposal, CERN/LHCC 94-43

12 E. Richter-Was, D. Froidevaux and J. Soderqvist, ATLAS Internal Note Phys-No-108

13 D. Froidevaux and E. Richter-Was, private communication

14 G. Polesello, transparencies from LHCC SUSY Workshop, October 1996, see http://atlasinfo.cern.ch/Atlas/GROUPS/PHYSICS/SUSY/susy.html

15 D. Froidevaux and E. Richter-Was, ATLAS Internal Note Phys-No-112

16 D. Froidevaux, transparencies from LHCC SUSY Workshop, October 1996, see http://atlasinfo.cern.ch/Atlas/GROUPS/PHYSICS/SUSY/susy.html

17 F. Gianotti et al., ATLAS Calorimeter Note in preparation